Effects of third-order dispersion on dispersion-managed solitons

T. I. Lakoba and G. P. Agrawal

Rochester Theory Center for Optical Science and Engineering, The Institute of Optics, P.O. Box 270186, University of Rochester, Rochester, New York 14627

Received January 1, 1999; revised manuscript received April 29, 1999

We present a comprehensive study of the effects of third-order dispersion (TOD) on dispersion-managed (DM) solitons. The two main effects of TOD are creation of asymmetry of the DM soliton's profile and generation of continuum radiation. Considering these two effects, we derive a conservative bound on the magnitude of TOD below which it will not have a significant detrimental effect on DM solitons over transoceanic distances. We also calculate the shifts in the DM soliton's position and central frequency that are due to TOD. Finally, we discuss a novel possibility of observing a nonradiating soliton in DM systems with TOD. © 1999 Optical Society of America [S0740-3224(99)00709-2]

OCIS codes: 060.5530, 060.2330, 190.4370.

1. INTRODUCTION

It has been shown in many recent studies (see, e.g., Refs. 1–14 and references therein) that the dispersion management technique can significantly improve the performance of soliton-based telecommunication systems. In its simple form, the dispersion management technique consists of using a periodic dispersion map such that each period is composed of two optical fibers of generally different lengths and opposite types of group-velocity dispersion (GVD). Such a dispersion map provides high GVD locally while keeping the average dispersion relatively low. The most advantageous regime appears to be that of strong dispersion management, for which the average GVD is much less than the local GVD. In this regime the effect of third-order dispersion (TOD) can become quite appreciable, especially as solitons become shorter with increasing bit rate. Surprisingly, the effect of TOD on dispersion-managed (DM) solitons has not yet been studied systematically. In Refs. 3 and 4 it was briefly mentioned that numerical simulations did not show splitting of a DM soliton when a sufficiently weak TOD was included. In experimental studies[5] it was noted that the average TOD in the dispersion map should be minimized by choice of fiber sections whose dispersion slopes (nearly) compensate for one another. References 6 and 7 presented numerical evidence that TOD can reduce long-term oscillations of a quasi-stationary DM soliton. The need to minimize the average TOD coefficient in nonsoliton dispersion-management systems was established in Ref. 8.

We present a comprehensive study of the effects of TOD on a single DM soliton. These effects are similar, with one exception, to the corresponding effects in the well-understood case of a uniform-dispersion fiber. Specifically, we find that the TOD (i) changes the DM soliton's velocity, (ii) leads to emission of continuum radiation by the soliton (see, e.g., Refs. 15–17 and references therein), and (iii) makes the soliton's shape asymmetric. We show that this asymmetry becomes more pronounced as the strength of the dispersion map increases. Moreover, we find that, in a fiber with periodically compensated loss, TOD leads to a continuous shift of the DM soliton's frequency. It should be emphasized that this frequency shift occurs only in fibers with both dispersion management and periodic compensation of the loss. In an idealized lossless fiber, or in a fiber with uniform dispersion, this shift vanishes.

The body of this paper is organized as follows: In Section 2 we present the generalized nonlinear Schrödinger (NLS) equation that governs the soliton evolution in optical fibers with both dispersion management and TOD. This equation is solved in Section 3 by use of an expansion of the DM soliton over a basis of Hermite–Gaussian (HG) components.[9,10] In Subsection 4.A we quantify the soliton's asymmetry by estimating the magnitude of its largest HG component that causes that asymmetry. Subsequently we derive an analytical bound on the TOD coefficient β_3 for which the energy of that HG component is not to exceed a certain small value, which we arbitrarily set to 1% of the total DM soliton energy. In Subsection 4.B we derive the expressions for the soliton position and frequency shifts. In Subsection 4.D we compare our analytical predictions with the results of direct numerical simulations. Subsection 4.C contains the main result of our study. First we show that, for the same value of β_3 that guarantees that the energy in the largest symmetry-breaking HG component is below the threshold chosen, the energy of the TOD-induced continuum radiation from the soliton is, in the generic case, still quite conspicuous. We then analyze how much further one should decrease β_3 to make the energy of the continuum radiation fall below the same threshold (for realistic distances of propagation). From these considerations we obtain a conservative upper bound on β_3 that can be tolerated in real systems. We emphasize that such a bound is generic. That is, there can be isolated values of β_3 for

0740-3224/99/091332-12$15.00

which the continuum is not generated, at least asymptotically for large propagation distances. This effect is in stark contrast to that for a uniform-dispersion fiber and occurs because of a special structure of the DM soliton's power spectrum. This issue is discussed in Section 5, where the summary of our results is also presented.

2. GENERALIZED NONLINEAR SCHRODINGER EQUATION

The basic equation that governs propagation of an optical pulse in a fiber and includes the effects of both the GVD and TOD can be written as[18]

$$i\left(\frac{\partial A}{\partial Z} + \beta_1\frac{\partial A}{\partial T}\right) - \frac{1}{2}\beta_2(Z)\frac{\partial^2 A}{\partial T^2} + \gamma|A|^2A - \frac{i}{6}\beta_3\frac{\partial^3 A}{\partial T^3} = \frac{i}{2}[g(Z) - \alpha]A, \quad (1)$$

where $\beta_m = (\mathrm{d}^m\beta/\mathrm{d}\omega^m)_{\omega=\omega_0}$ with $m = 1, 2, 3$ to take into account dispersive effects at progressively higher orders. Physically, $\beta_1 \equiv 1/v_g$ is inversely related to the group velocity, and β_2 is called the GVD parameter because it takes into account the dispersion of the group velocity. The effects of TOD are included through β_3. Parameters β_2 and β_3 are related to the dispersion coefficient D and its slope $\mathrm{d}D/\mathrm{d}\lambda$ by

$$\beta_2 = -\frac{\lambda^2}{2\pi c}D, \qquad \beta_3 = \left(\frac{\lambda^2}{2\pi c}\right)^2\left(\frac{2D}{\lambda} + \frac{\mathrm{d}D}{\mathrm{d}\lambda}\right), \quad (2)$$

where λ is the operating wavelength and c is the speed of light. For most fibers, the first term in the expression for β_3 is much less than the second term, whence

$$\beta_3 \approx \left(\frac{\lambda^2}{2\pi c}\right)^2\frac{\mathrm{d}D}{\mathrm{d}\lambda}. \quad (2')$$

Parameter γ in Eq. (1) is the nonlinearity coefficient, and the effect of fiber loss and its periodic compensation is included through the parameters α and $g(z)$, respectively. Varying the form of α and $g(z)$, we can study the case of an idealized lossless fiber as well as the cases of lumped and distributed amplification. In a DM fiber, $\beta_2(Z)$ is a piecewise-constant, periodic function with values β_{21} and β_{22} in the two sections of the dispersion map. The lengths of these two sections are L_1 and L_2, respectively, and $L_1 + L_2 = L_{\mathrm{map}}$, where L_{map} is the period of the map.

It is common to introduce normalized variables and write Eq. (1) in a dimensionless form. We introduce new variables as

$$z = Z/L_{\mathrm{map}}, \qquad \tau = (T - \beta_1 Z)/T_{\mathrm{DM}},$$
$$u = A\exp\left[1/2\int_0^Z g(Z')\mathrm{d}Z' - 1/2\alpha Z\right]\Big/\sqrt{P_0}, \quad (3)$$

where T_{DM} is a time-scaling parameter chosen such that

$$T_{\mathrm{DM}} = (|\beta_{21} - \beta_{22}|L_1L_2/L_{\mathrm{map}})^{1/2}. \quad (4)$$

Parameter P_0 is a reference power used for normalization and equals the peak power in a lossless fiber. Its relation to the average pulse power or to the pulse energy in a fiber with periodically compensated loss is specified after Eq. (14) below.

In terms of the normalized variables z, τ, and u we obtain the following nondimensional form of the NLS equation:

$$i\frac{\partial u}{\partial z} + \frac{1}{2}D(z)\frac{\partial^2 u}{\partial \tau^2} + \epsilon\left[\frac{1}{2}D_0\frac{\partial^2 u}{\partial \tau^2} + G(z)|u|^2u\right] = i\mu\epsilon\frac{\partial^3 u}{\partial \tau^3}, \quad (5)$$

where the periodic coefficient

$$G(z) = \exp\{L_{\mathrm{map}}[\textstyle\int_0^z g(z')\mathrm{d}z' - \alpha z]\}$$

accounts for weakening of the nonlinear effects as a result of the fiber loss. The dimensionless parameters ϵ and μ are defined as

$$\epsilon = \gamma P_0 L_{\mathrm{map}}, \qquad \mu = \beta_3/(6\gamma P_0 T_{\mathrm{DM}}{}^3). \quad (6)$$

The average GVD, ϵD_0, is introduced through

$$\epsilon D_0 = -\frac{(\beta_{21}L_1 + \beta_{22}L_2)L_{\mathrm{map}}}{|\beta_{21} - \beta_{22}|L_1L_2}, \quad (7)$$

whereas the periodic part of the GVD coefficient, $D(z)$, in each period of the dispersion map varies as

$$D(z) = \begin{cases} \mathrm{sgn}(\beta_{22} - \beta_{21})L_{\mathrm{map}}/L_1 & 0 < z < L_1/L_{\mathrm{map}} \\ -\mathrm{sgn}(\beta_{22} - \beta_{21})L_{\mathrm{map}}/L_2 & L_1/L_{\mathrm{map}} < z < 1 \end{cases}. \quad (8)$$

The local GVD, $D(z)$, is assumed to be much greater than both the average GVD, ϵD_0, and the nonlinearity, which implies that $\epsilon \ll 1$. Thus, in the absence of TOD, the strong local GVD determines the functional form of the DM soliton's shape (see below), and the weaker average GVD and nonlinearity provide the relation between the amplitude and the width of a stationarily propagating soliton. To carry out the perturbation theory when TOD is included, we assume that its effect on the DM soliton is even smaller than that of the average GVD and nonlinearity and thus require that $\mu \ll 1$. This condition holds in most practical situations. Although we take μ to be a constant, our results can easily be generalized to the case in which μ is different in the two sections of the dispersion map by simply replacing μ by its weighted average value, $(\mu_1L_1 + \mu_2L_2)/L_{\mathrm{map}}$, in the two sections.

3. HERMITE–GAUSSIAN EXPANSION

In this section we solve Eq. (5), using the HG expansion introduced in Refs. 9 and 10 (see also Ref. 12). This approach is based on the analytical solution of Eq. (5) that is easy to obtain when $\epsilon = 0$ and includes the effects of ϵ-dependent terms as a perturbation. We first set $\mu = 0$ and review those results obtained in Ref. 12 that are relevant to the present study. When $\mu = 0$ and $\epsilon \ll 1$, a DM soliton can be represented as the following superposition of chirped HG components:

$$u_0 = \sum_{n=0}^{\infty} \frac{a_n}{\sqrt{1 + i\delta}} \left(\frac{1 - i\delta}{1 + i\delta} \right)^{n/2} H_n(\xi) \times \exp\left[-\frac{\xi^2}{2}(1 - i\delta) - i\omega_0 \tau_0 \sqrt{1 + \delta^2}\,\xi + i\phi(z) \right] + O(\epsilon), \tag{9}$$

where $H_n(\xi)$ are the Hermite polynomials,

$$\delta \equiv \delta(z) = \delta_0 + \frac{1}{\tau_0^2} \int_0^z D(z')\mathrm{d}z',$$

$$\xi = \frac{\tau - \tau_c(z)}{\tau_0 \sqrt{1 + \delta^2}}, \tag{10}$$

τ_0 is the minimum pulse width and occurs at values of z for which $\delta(z) = 0$, and ω_0 is the frequency shift of the soliton spectrum from the carrier frequency. The center $\tau_c(z)$ of the soliton and its phase $\phi(z)$ evolve with propagation according to the following two equations:

$$\frac{\mathrm{d}\tau_c}{\mathrm{d}z} = -\omega_0 [D(z) + \epsilon D_0], \tag{11}$$

$$\frac{\mathrm{d}\phi}{\mathrm{d}z} = \frac{\omega_0^2}{2}[D(z) + \epsilon D_0] + \epsilon \frac{|a_0|^2}{\sqrt{2}} \left(I_0 - \frac{I_2}{4} \right) + O(\epsilon^2), \tag{12}$$

where I_0 and I_2 are obtained from

$$I_n = \int_0^1 \frac{\mathrm{d}z G(z)}{\sqrt{1 + \delta^2}} \left(\frac{1 + i\delta}{1 - i\delta} \right)^{n/2}, \qquad n = 0, 1, 2, \ldots. \tag{13}$$

The nature of the terms collectively denoted $O(\epsilon)$ in Eq. (9) is different from that of the ϵ-order terms in Eqs. (11) and (12). According to the method of multiple scales, by which solution (9) was obtained in Ref. 12, the former group of terms represents small oscillatory corrections to the zeroth-order solution, whereas the latter group yields ϵ-order corrections to the evolutions of the pulse parameters.

In Eq. (9) we have included the frequency parameter ω_0 for the sake of completeness only. In the case of a single channel, we can always take $\omega_0 = 0$. Moreover, even in the presence of TOD (i.e., when $\mu \neq 0$), a nonzero ω_0 can be eliminated by a well-known transformation in Eq. (5) (see, e.g., Ref. 19):

$$z \to \bar{z} = z,$$

$$\tau \to \bar{\tau} = \tau + [(\delta \tau_0^2 + \epsilon D_0 z)\omega_0 - 3\epsilon\mu\omega_0^2 z],$$

$$u \to \bar{u} = u \exp\{i[\omega_0 \tau - \mu\epsilon z \omega_0^3 + \omega_0^2(\delta\tau_0^2 + \epsilon D_0 z)/2]\},$$

$$D_0 \to \bar{D}_0 = D_0 - 6\mu\omega_0.$$

For this reason, below we shall consider solution (9) with $\omega_0 = 0$. However, a frequency shift $\mathrm{d}\omega_0/\mathrm{d}z$ can still be nonzero.

We can determine the amplitudes a_n in Eq. (9) by substituting expansion (9) into Eq. (5). When $\mu = 0$, all HG components with odd n vanish. Moreover, the amplitudes a_n of even terms decrease rapidly with increasing n. Therefore, as the first approximation, we can consider the evolution of just the two lowest-order amplitudes, a_0 and a_2. If a_2 is found to exhibit any significant growth, the DM soliton will lose its single-peak structure; i.e., it will be destroyed. The requirement that no such growth of a_2 occur leads to the following two relations[9,11]:

$$|a_0|^2 = D_0 \sqrt{2}/(\tau_0^2 \,\mathrm{Re}\, I_2), \qquad \mathrm{Im}\, I_2 = 0. \tag{14}$$

Under these conditions and within the two-component approximation, we also find that $a_2 = 0$, and hence a_0 is the amplitude of the DM soliton. This amplitude can always be normalized to unity by a proper choice of P_0, in which case the average soliton power is just $P_0 I_0$. Alternatively, the DM soliton energy immediately after an amplifier equals $\sqrt{\pi} G(z_{\mathrm{amp}}) P_0 T_{\mathrm{DM}} \tau_0$, where $G(z_{\mathrm{amp}})$ is the value of $G(z)$ at the amplifier's location. In what follows, we do not set a_0 to unity but keep it arbitrary, because the resultant formulas then show explicit dependence on the soliton power.

We now consider the effects of TOD on the DM soliton. When $\mu \neq 0$, the TOD is expected to generate HG components with odd n in Eq. (9), making the coefficients a_1, a_3, etc. nonzero. One can always reduce the $n = 1$ component to zero by readjusting the parameters τ_c and ω_0 of the soliton.[12] Thus the lowest HG component that would contribute to the soliton's asymmetry is the $n = 3$ component. We point out that there could, in principle, exist stationary, weakly asymmetric DM solitons supported by a delicate balance among nonlinearity, average GVD, and TOD. Moreover, as we show in Section 5 below, such weakly asymmetric DM solitons do exist. However, the relative amplitudes of the third- and higher-order HG components in such solitons should be sufficiently small. Otherwise, if the TOD-induced third HG component becomes large enough, conspicuous higher-order components will be generated through the nonlinearity. A pulse with many excited HG components will no longer keep its single-peak structure. In fact, it can be destroyed, although it is not known exactly how much energy in the components with $n > 0$ a DM soliton can tolerate. On the other hand, if the TOD-induced third HG component remains sufficiently small, the higher-order components will also remain small, and the DM soliton should be stable. Thus we proceed to obtain a generic condition on β_3 that will keep the amplitude a_3 of the third HG component below some small value.

As before, we begin by substituting Eq. (9) into Eq. (5) and collecting the coefficients for each HG component. To the first order in ϵ, a μ-dependent term is added to each equation in the infinite set of equations obtained in Ref. 12. In particular, the coefficient a_n satisfies

$$i\dot{a}_n + [\text{as in Ref. 12}] = \frac{i\mu}{\tau_0^3}[(n+1)(n+2)(n+3)a_{n+3} - {}^3\!/_2 (n+1)^2 a_{n+1} + {}^3\!/_4 n a_{n-1} - {}^1\!/_8 a_{n-3}], \tag{15}$$

where the overdot denotes the derivative with respect to the slow variable (ϵz).

We cannot solve the infinite set of equations obtained above in a closed form without making further approximations. Recall that, in the absence of TOD ($\mu = 0$), the consideration of just the first two even HG components was sufficient to provide conditions (14) for the DM soliton's parameters, whereas components with $n \geqslant 4$ led only to small corrections.[10,12] Therefore we expect that the consideration of the first four components with $n = 0-3$ will provide us with a good approximation of the results that we seek. This truncation of the infinite set of equations to just four equations reduces the complexity of the problem considerably. Inasmuch as we are interested only in the asymptotic behavior that occurs for $z \to \infty$, we set $\dot{a}_n = 0$ for $n = 0-3$. Thus we neglect the effect of the continuum radiation on the DM soliton and assume that a weakly asymmetric DM soliton is formed at $z \to \infty$. Next, as shown in Ref. 12, we can always adjust the soliton's parameters τ_c, ω_0, τ_0, and δ_0 to have $a_1 = a_2 = 0$. Moreover, we can set a_0 to be purely real without loss of generality. As a final simplification, we carry out the analysis of the truncated system only to the first order in μ. Because for $\mu = 0$ there is no third HG component in the DM soliton ($a_3 = 0$) and the parameters ω_0 and τ_c are constant, we assume that for $\mu \ll 1$ they all vary as

$$|a_3| \sim \dot{\tau}_c \sim \dot{\omega}_0 \sim \mu. \tag{16}$$

We should still enforce the condition $\dot{\tau}_0 = \dot{\delta}_0 = 0$ to prevent the pulse's spread or collapse. However, we shall allow conditions (14) to be violated by an amount $O(\mu)$.

The equation for $n = 0$ in the set of four equations obtained from Eq. (15) with $n = 0-3$ is automatically satisfied to the first order in μ. The remaining three equations for $n = 1, 2, 3$ with the above simplifications can be written, respectively, as

$$3a_3\left(\frac{D_0}{{\tau_0}^2} - \frac{{a_0}^2 I_{-2}}{\sqrt{2}}\right) - a_3^*\left(\frac{3{a_0}^2 I_4}{2\sqrt{2}}\right) - a_0\left(\frac{3i\mu}{4{\tau_0}^3} - \frac{\dot{\omega}_0\tau_0}{2} - \frac{i\dot{\tilde{\tau}}_c}{2\tau_0}\right) = 0, \tag{17a}$$

$$\frac{D_0}{{\tau_0}^2} = \frac{{a_0}^2 I_2}{\sqrt{2}}, \tag{17b}$$

$$-a_3\left(\frac{3D_0}{2{\tau_0}^2} + \frac{3{a_0}^2 I_0}{8\sqrt{2}}\right) + a_3^*\left(\frac{5{a_0}^2 I_6}{16\sqrt{2}}\right) + a_0\left(\frac{i\mu}{8{\tau_0}^3}\right) = 0, \tag{17c}$$

where[12]

$$\dot{\tilde{\tau}}_c = \dot{\tau}_c + \dot{\omega}_0[\mathrm{sgn}(\beta_{22} - \beta_{21})/2 + \delta_0{\tau_0}^2]. \tag{18}$$

From Eq. (17) we immediately see that TOD does not modify conditions (14). Also, because I_2 is real, we have that $I_2 = I_{-2}$, and hence the first term in Eq. (17a) vanishes. From Eq. (17c) we can find $a_3 = a_{3R} + ia_{3I}$ in terms of a_0. The result is

$$\frac{a_{3R}}{a_0} = \frac{5\mu I_{6I}}{\sqrt{2}{\tau_0}^3{a_0}^2[(3I_0 + 12I_2)^2 - (5/2|I_6|)^2]}, \tag{19a}$$

$$\frac{a_{3I}}{a_0} = \frac{\sqrt{2}\mu(3I_0 + 12I_2 - 5/2I_{6R})}{{\tau_0}^3{a_0}^2[(3I_0 + 12I_2)^2 - (5/2|I_6|)^2]}. \tag{19b}$$

Finally, from Eq. (17a) we find that the soliton's frequency and the center position change linearly with z, and the rate of change in terms of the previously defined quantities is given by

$$\dot{\omega}_0 = \frac{3{a_0}^2}{\sqrt{2}\tau_0}\left(\frac{a_{3R}}{a_0}I_{4R} + \frac{a_{3I}}{a_0}I_{4I}\right), \tag{20}$$

$$\dot{\tilde{\tau}}_c = \frac{3\mu}{2{\tau_0}^2} + \frac{3{a_0}^2\tau_0}{\sqrt{2}}\left(\frac{a_{3R}}{a_0}I_{4I} - \frac{a_{3I}}{a_0}I_{4R}\right) \tag{21}$$

[recall that the overdot denotes the slow derivative, $\mathrm{d}/\mathrm{d}(\epsilon z)$]. This completes the formal solution of Eq. (5) to the first order in the TOD parameter μ. Assuming that the DM soliton, found when $\mu = 0$, remains an approximate solution even when $\mu \neq 0$, we have shown that its frequency and position change linearly with propagation, with the rates of change being proportional to μ. At the same time, the creation of the third HG component makes the soliton shape asymmetric.

4. EFFECTS OF THIRD-ORDER DISPERSION

In this section we use the results of the preceding section to study the effects of TOD on the DM soliton. In general, we need to specify a large number of parameters related to the dispersion map and the input pulse launched into the fiber. However, when the nonlinearity and the average GVD are small (i.e., $\epsilon \ll 1$), the results of previous studies indicate that the single most important parameter is the normalized pulse width $\tau_0 = T_0/T_{\mathrm{DM}}$. Here T_0 is the minimum width of the Gaussian pulse, related to the full width at half-maximum (FWHM) as $T_{\mathrm{FWHM}} = 2\sqrt{\ln 2}T_0$. For convenience and for easy comparison with previous studies we use a related dimensionless parameter S, called the strength of the dispersion map and defined as follows:

$$S = \frac{1}{2{\tau_0}^2} = \frac{2\ln 2|\beta_{21} - \beta_{22}|L_1L_2}{L_{\mathrm{map}}{T_{\mathrm{FWHM}}}^2} = \ln 2\,\frac{|(\beta_{21} - {\beta_2}^{\mathrm{av}})L_1 - (\beta_{22} - {\beta_2}^{\mathrm{av}})L_2|}{{T_{\mathrm{FWHM}}}^2}, \tag{22}$$

where ${\beta_2}^{\mathrm{av}} = (\beta_{21}L_1 + \beta_{22}L_2)/L_{\mathrm{map}}$. Except for a factor of $\ln 2 \approx 0.69$, our definition of S agrees with that of Ref. 2. Stationary propagation of a DM soliton at zero average GVD requires a specific value $S = S_0$, where the quantity $\mathrm{Re}\,I_2$ vanishes [cf. Eqs. (14)]. Accordingly, the average GVD should be normal for $S > S_0$. For both lossless and periodically amplified cases, the value of S_0 was found[13] to be approximately equal 3.3. Note that when we consider higher-order corrections in ϵ (i.e., the high-power regime) we find that for $S > S_0$ the DM soliton can exist for either sign of the average

GVD.[4,14] In the present study we restrict the consideration to the low-power regime, for which conditions of stationary propagation are given by Eqs. (14).

A. Asymmetry of the Dispersion-Managed Soliton

The presence of the $n = 3$ component in Eq. (9) shows that the shape of the DM soliton is no longer symmetric. The magnitude of the $n = 3$ component is governed by the coefficient a_3 that is generally complex. Consider first the ideal case of a lossless fiber by setting $\alpha = g(z) = 0$. As $G(z) = 1$ in this case, all integrals I_n are functions only of S. Moreover, the condition $\mathrm{Im}\, I_2 = 0$ in Eqs. (14) guarantees that $\delta_0 = -\mathrm{sgn}(\beta_{22} - \beta_{21})/2\tau_0^2$, ensuring that all I_n with even n are real.[12] It follows from Eq. (19a) that $a_{3R} = 0$; i.e., a_3 is purely imaginary. The relative magnitude of the third HG component is then obtained from Eq. (19b) and is given by

$$\left|\frac{a_3}{a_0}\right| = \frac{2(2\ln 2)^{3/2}|\beta_3|}{3\gamma(P_0 a_0^2)T_{\mathrm{FWHM}}^3}\left(\frac{1}{3I_0 + 12I_2 + 5/2I_6}\right). \quad (23)$$

The factor within the large parentheses depends on the dispersion map strength S and increases rapidly with increasing S (see below). As we discussed at length in the paragraph following Eqs. (14), we need to keep the quantity $|a_3/a_0|$ sufficiently small if the DM soliton is going to survive the TOD-induced degradation. We use the criterion that the energy in the third HG component does not exceed 1% of the total soliton energy, with the latter being approximately equal to the energy in the zeroth HG component. Using Eq. (23), the definition of energy $E \equiv \int_{-\infty}^{\infty}|u|^2 d\tau$, and the normalization condition for Hermite polynomials:

$$\int_{-\infty}^{\infty} H_n^2(x)\exp(-x^2)dx = 2^n n!\sqrt{\pi}, \quad (24)$$

we obtain the following condition:

$$\frac{\beta_3}{\gamma P_{\mathrm{av}} T_{\mathrm{FWHM}}^3} \equiv \frac{L_{\mathrm{NL}}}{L_{\mathrm{TOD}}} \leqslant \frac{9}{2(2\ln 2)^{3/2}}\frac{0.1}{\sqrt{48}}\left(1 + 4\frac{I_2}{I_0} + \frac{5}{6}\frac{I_6}{I_0}\right), \quad (25)$$

where $P_{\mathrm{av}} = P_0 a_0^2 I_0$ and L_{NL} and L_{TOD} are, respectively, the nonlinear and the TOD length scales defined by the relations

$$L_{\mathrm{TOD}} = \frac{T_{\mathrm{FWHM}}^3}{|\beta_3|}, \qquad L_{\mathrm{NL}} = \frac{1}{\gamma P_{\mathrm{av}}}. \quad (26)$$

In what follows, we denote by $\beta_3^{1\%}$ the value of β_3 for which the equality in expression (25) holds. Clearly, this value depends on the pulse power and width and on the DM strength S. Below, we explicitly indicate only the last dependence by writing $\beta_3^{1\%} = \beta_3^{1\%}(S)$. Numerical verification of expression (25) is discussed in Subsection 4.C below.

In practice, fibers are always lossy, and their loss is compensated for periodically by use of in-line amplifiers. In that case, $G(z) = [\alpha L_{\mathrm{amp}}/(1 - \exp(-\alpha L_{\mathrm{amp}})] \times \exp(-\alpha z)$ within one amplification span and is repeated periodically with the period L_{amp}. The prefactor in front of $\exp(-\alpha z)$ ensures the condition $\int_0^1 G(z)dz = 1$. Given the explicit form of $G(z)$, the integrals I_n in Eq. (13) can be evaluated numerically (cf. Refs. 12 and 13). The resultant threshold value of $L_{\mathrm{NL}}/L_{\mathrm{TOD}}$ can then readily be calculated from Eqs. (19) as a function of S. As an example, in Fig. 1 we plot the threshold value of $L_{\mathrm{NL}}/L_{\mathrm{TOD}}$ as a function of S, using $\alpha = 0.22$ dB/km for three different periodic amplification schemes considered previously in Ref. 13. In all three cases the amplifier spacing and the dispersion-map period are the same and are equal to 40 km. Curves (b) and (c) of Fig. 1 correspond to postcompensation and precompensation ($L_1/L_{\mathrm{map}} = 0.9$ and $L_1/L_{\mathrm{map}} = 0.1$), respectively. Because they are very close to each other, in Fig. 1 we show only one of them. Curve (d) corresponds to the case $L_1/L_{\mathrm{map}} = 7/18$, for which the energy enhancement factor was found to be maximum for any given value of S in the range 0–3.3.[13] The lossless case is shown by curve (a). Because curves (a) and (d) are very close to each other (which is in agreement with the observation in Ref. 13 that the periodically compensated case with $L_1/L_{\mathrm{map}} = 7/18$ is in many respects similar to the lossless case), we also show only one of them in Fig. 1.

The main conclusion that follows from Fig. 1 is that $\beta_3^{1\%}$ decreases as the map strength increases. We now consider an example whose purpose is to illustrate how our criterion [expression (25)] can be applied to a practical system. Consider a DM soliton with $T_{\mathrm{FWHM}} = 8$ ps and $P_{\mathrm{av}} = 2$ mW, propagating at $\lambda = 1550$ nm in a map that consists of the longer segment of the Corning LEAF dispersion-shifted fiber (DSF) with $D_{\mathrm{DSF}} = 4$ ps/(nm km), $dD/d\lambda = 0.11$ ps/(nm^2 km), $\alpha = 0.21$ dB/km, and effective core area $A_{\mathrm{eff}} = 72\,\mu\mathrm{m}^2$ and of the shorter segment of dispersion-compensating fiber (DCF) with $D_{\mathrm{DCF}} = -100$ ps/(nm km). We take the map period to be $L_{\mathrm{map}} = 33$ km. Below, we determine the maximum value of $dD_{\mathrm{DCF}}/d\lambda$ required for the inequality in expression (25) to hold. As long as the average GVD is much

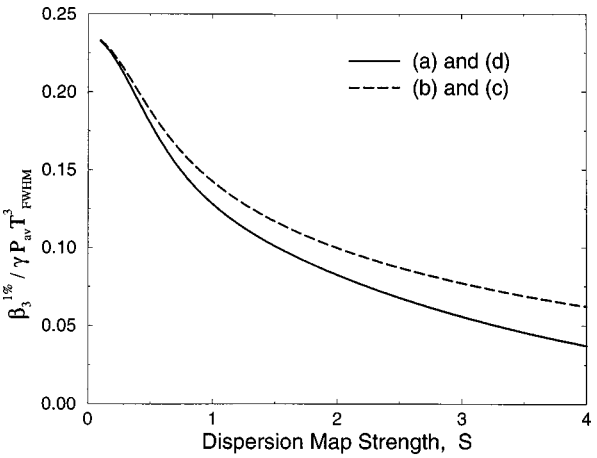

Fig. 1. Normalized value of the TOD coefficient for which the energy in the third HG component equals 1% of the total DM soliton energy, plotted as a function of map strength S. (a) Lossless case; (b), (c), (d), periodically amplified case with $\alpha = 0.22$ dB/km, $L_{\mathrm{map}} = L_{\mathrm{amp}} = 40$ km, and $L_1/L_{\mathrm{map}} = 0.9$, 0.1, 7/18, respectively.

smaller than the local GVD, the length of the DCF is much smaller than that of the DSF, and hence the attenuation and the nonlinearity of the DCF can be neglected. For the parameters specified above, we have $L_{\mathrm{DSF}} \approx 31.7\,\mathrm{km}$ and $L_{\mathrm{DCF}} \approx 1.3\,\mathrm{km}$. Then the dispersion management strength is estimated from Eqs. (22) and (2) to be $S \approx 3.5$. The nonlinearity coefficient is found from $\gamma = 2\pi n_2/(\lambda A_{\mathrm{eff}})$, where $n_2 \approx 3 \times 10^{-20}\,\mathrm{m^2/W}$,[18] to be $\gamma \approx 1.7\,(\mathrm{km\,W})^{-1}$. Now the parameters of the considered map are rather close to those for which curve (b) of Fig. 1 is obtained, and we verified that the threshold values ${\beta_3}^{1\%}(S)$ are also close in these two cases. Hence we use the threshold value ${\beta_3}^{1\%}$ from Fig. 1, along with expression (25) and relation (2′), to find the maximum allowed average value of the dispersion slope to be $(\mathrm{d}D/\mathrm{d}\lambda)_{\mathrm{av}} \approx 0.097\,\mathrm{ps/(nm^2\,km)}$. This implies that the maximum allowed value for $\mathrm{d}D_{\mathrm{DCF}}/\mathrm{d}\lambda$ in such a dispersion map is $-0.22\,\mathrm{ps/(nm^2\,km)}$. Conversely, given the actual dispersion slope of the DCF segment, we could have verified whether the inequality in expression (25) holds for the resultant dispersion map.

B. Temporal and Spectral Shifts

In the lossless case, all integrals I_n with even n are real, as we explained above. Inasmuch as $a_{3R} = 0$ in that case, then from Eq. (20) we have $\dot{\omega}_0 = 0$. Thus, in a lossless fiber, the TOD will not shift the soliton's frequency in the approximation used here. However, its position will still shift according to Eq. (21). With $a_{3R} = 0$ and inasmuch as I_4 and I_6 are real, the temporal shift in physical units, $T_c = \tau_c T_{\mathrm{DM}}$, is given by

$$T_c(Z) = \frac{(\ln 2)\beta_3 Z}{{T_{\mathrm{FWHM}}}^2}\left(1 - \frac{2I_4}{3I_0 + 12I_2 + 5/2I_6}\right). \quad (27)$$

The first term within large parentheses in Eq. (27) comes from eliminating the first HG component by setting $a_1 = 0$; the second term is a contribution of the third HG component [see Eq. (21)]. The factor within the large parentheses is close to 1 and increases from 0.88 to 1.14 only when the map strength S increases from 0 to 3.3 (where $D_0 \approx 0$). Thus the contribution of the third HG component to the shift of the soliton's position is relatively small (within ±15%), and we conclude that the TOD-induced shift in the soliton position is nearly independent of the dispersion management strength. As an estimate, the position shifts at a rate of ~3 fs/km if we use $\beta_3 = 0.1\,\mathrm{ps^3/km}$ [$\mathrm{d}D/\mathrm{d}\lambda \approx 0.06\,\mathrm{ps/(nm^2\,km)}$ at $\lambda = 1550$ nm] and $T_{\mathrm{FWHM}} = 5$ ps as typical values. Even such a small shift would become noticeable after the soliton propagated over a transoceanic distance.

When the fiber loss is included, the major difference is that I_n for even n are no longer real. It follows from Eq. (19a) that $a_{3R} \neq 0$. As a result, both terms in Eq. (20) become nonzero and lead to a frequency shift of the DM soliton that increases linearly with z. The conclusions about the soliton's position shift for the periodically amplified case remain qualitatively the same as in the lossless case and thus are not discussed further. The rate of the normalized frequency shift, $\dot{\omega}_0\tau_0/I_0 = 2\sqrt{\ln 2}L_{\mathrm{NL}}(\mathrm{d}\nu/\mathrm{d}Z)/\Delta\nu_{\mathrm{FWHM}}$, is plotted in Fig. 2 versus the dispersion map strength S [curves (b)–(d)] for the same three values of L_1/L_{map} as in Fig. 1. Curve (a) of Fig. 2 corresponds to the frequency shift that occurs because of the spectral recoil effect in a lossless fiber and is discussed below.

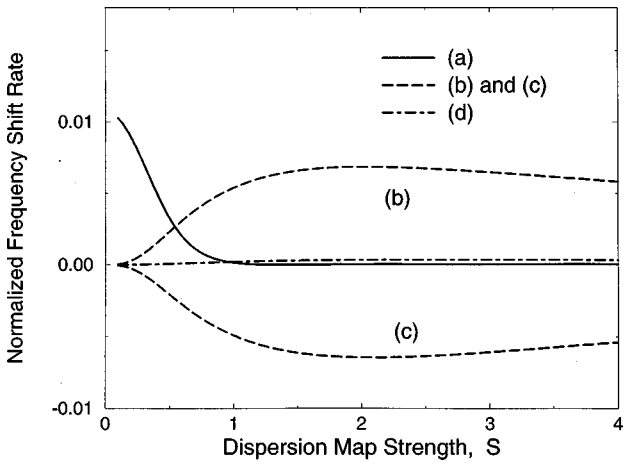

Fig. 2. Rate of the normalized frequency shift $\dot{\omega}_0\tau_0/I_0$ that occurs as the result (a) of spectral recoil in a lossless fiber and (b)–(d) of generation of a third HG component of a DM soliton in a periodically amplified DM fiber. Parameters for (b)–(d) are the same as in Fig. 1.

Note that we set $\beta_3 = {\beta_3}^{1\%}(S)$ in all cases shown in Fig. 2, which ensures that the energy in the third HG component will remain sufficiently small and that the pulse will be almost undistorted. In fact, this smallness of the third HG component guarantees that the frequency shift associated with the creation of this component will also be quite small. Indeed, it follows from the behavior of curves (b) and (c) of Fig. 2 that even when $L_1/L_{\mathrm{map}} = 0.1$ or $L_1/L_{\mathrm{map}} = 0.9$ and for $S \approx 1.8$, where the frequency shift is the most conspicuous, the DM soliton's central frequency shifts by $\Delta\nu_{\mathrm{FWHM}}$ after propagation over a distance of more than $140L_{\mathrm{NL}}$. Because in the strong DM regime $L_{\mathrm{NL}} \gg L_{\mathrm{map}}$ and L_{map} is a few tens of kilometers, we conclude that this frequency shift can be negligible, provided that we enforce the condition $\beta_3 \leqslant {\beta_3}^{1\%}(S)$.

C. Numerical Verification of Expression (25)

To verify the validity of the approximate analytical results obtained in Subsection 4.A, we solve Eq. (5) numerically. In all numerical simulations we choose $\epsilon = 0.2$, $G(z) = 1$ (lossless fiber) and $L_1 = L_2 (= 0.5)$. The initial soliton, launched with an appropriate chirp at the beginning of the anomalous section, was taken as a superposition of the two HG components with $n = 0$ and $n = 4$:

$$u_0 = \left[a_0 + a_4\left(\frac{1 - i\delta_0}{1 + i\delta_0}\right)^2 H_4(\tau/\tau_i)\right] \times \exp\left[-\frac{\tau^2}{2{\tau_i}^2}(1 - i\delta_0)\right], \quad (28)$$

where $\tau_i = (1 + {\delta_0}^2)/\sqrt{2S}$, $a_0 = 1$, and a_4 was taken according to the equation presented in Refs. 9 and 12. Once we specify the minimum pulse width τ_0 or, equivalently, the dispersion management strength S

$= 1/(2\tau_0^2)$, the initial chirp δ_0 and the average GVD ϵD_0 are set according to Eqs. (14). (We even included higher-order corrections that are due to the $n = 4$ HG component[12] for improved accuracy, although this was not found to have any major effect on our results.)

In Fig. 3 we plot the evolution with z of the ratio of the energies of the third and zeroth HG components of a DM soliton affected by TOD. The two curves in Fig. 3 correspond to the dispersion management strength values of $S = 1$ and $S = 3$ (recall that $D_0 = 0$ at $S \approx 3.3$). In both cases the dimensionless TOD parameter μ was taken to be $\mu = \mu^{1\%}(S)$, where $\mu^{1\%}(S)$ is computed from Eq. (6) for $\beta_3 = \beta_3{}^{1\%}(S)$. For $S = 1$ the numerical results are in good agreement with the analytically calculated asymptotic limit of 1% for the energy ratio. Inasmuch as the expression for a_3 in Section 3 was obtained in the limit $z \to \infty$, the large burst of $|a_3|$ near $z = 30$ seen in Fig. 3 is not accounted for by our theory. For $S = 3$ the agreement is less satisfactory, as the asymptotic value of the energy ratio is ~0.006. (Note, however, that the corresponding ratio of the amplitudes is ~0.077, i.e., is lower than the analytical result by less than 25%.) In this regard we also recall that our very choice of the threshold for the ratio of the third and zeroth HG components to equal 1% is itself rather arbitrary, and hence a deviation from it by a factor of order unity should be of little consequence for the dynamics of the DM soliton. Moreover, in Subsection 4.D we show that generation of continuum radiation by the DM soliton can be a stronger effect than generation of the third HG component. Nevertheless, the quantity $\beta_3{}^{1\%}(S)$ defined above is still found to provide a useful reference for quantifying the effect of TOD on a DM soliton.

D. Generation of Continuum Radiation

The preceding analysis does not include the generation of continuum radiation by the DM soliton perturbed by TOD. How important is this effect compared with the generation of the third HG component? It is well known (see, e.g., Ref. 17 and references therein) that a NLS soliton, when it is perturbed by TOD, generates dispersive

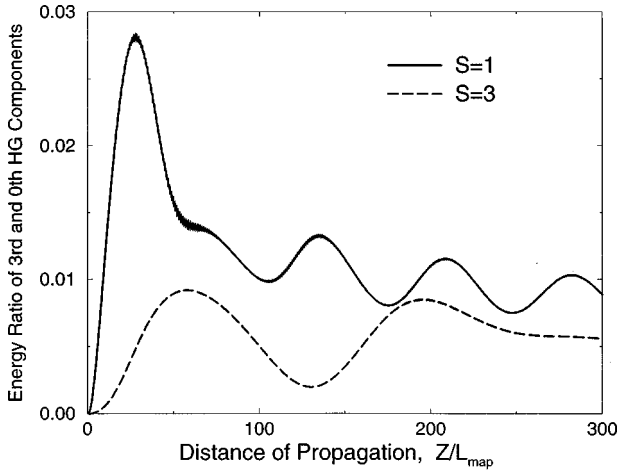

Fig. 3. Evolution of the ratio of the energies of the third and zeroth HG components for $S = 1$ and $S = 3$. In both cases, $\mu = \mu^{1\%}(S)$. Other parameters are specified in the text.

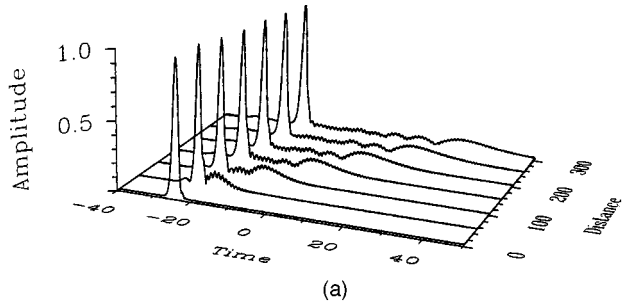

(a)

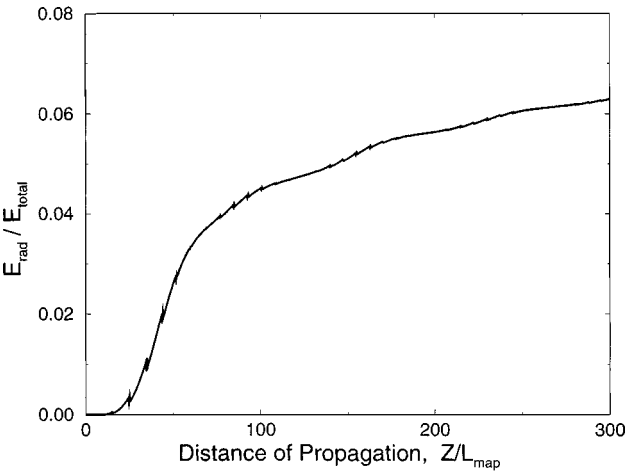

(b)

Fig. 4. Evolution over $300L_{\text{map}}$ (a) of the pulse amplitude and (b) of the ratio of the radiation energy to the total DM soliton energy for $S = 1$ and $\mu = \mu^{1\%}$. Other parameters are specified in Subsection 4.C.

waves into a shelf that propagates away from the soliton. A similar situation also occurs for a DM soliton. In Fig. 4(a) we plot the evolution of the DM soliton profile found numerically from Eq. (5) for a representative case of a lossless fiber and dispersion management strength $S = 1$. The other parameters in this simulation are as in Subsection 4.C. The formation of a shelf behind the soliton, consisting of continuum radiation emitted at a frequency different from that of the soliton, is clearly seen in Fig. 4(a). For a stronger map with $S = 3$ we observed a similar behavior, except that the shelf length increased approximately four times slower than it did for $S = 1$. This result agrees with the equation for the shelf length as found after Eq. (A6) in Appendix A. In Fig. 4(b) we plot, for $S = 1$ only, the energy contained in the shelf as a function of the propagation distance. The important conclusion of Fig. 4(b) is as follows: Whereas for $\beta_3 = \beta_3{}^{1\%}$ the energy of the third HG is 1% of the total soliton energy, the energy of the continuum radiation is several times larger. Thus, for $\beta_3 = \beta_3{}^{1\%}$, the continuum radiation is the dominant effect produced by TOD.

There are, in principle, standard methods[15–17,20] that allow this radiation field to be calculated asymptotically for large z. However, as we now explain, these methods can give only an order-of-magnitude estimate in the case in which we are interested. For a transoceanic distance of a few thousand kilometers and the typical value of $L_{\text{map}} \sim 50$ km, the dimensionless distance $z = Z/L_{\text{map}}$ is less than 300. As we can see from Fig. 4(b), the evolution

of the radiation consists of two distinct stages. In the first stage, associated with the formation of the shelf's head clearly seen in Fig. 4(a), the radiation energy increases rapidly. (The formation of the shelf's head was also noted in Refs. 20 and 21 for a NLS soliton affected by TOD.) Then, for larger distances, when a relatively flat shelf begins to form, the energy increase becomes slower and almost linear in z. It is this second stage that is described by the asymptotic methods of Refs. 15–17 and 20. However, for $z < 300$, the energy generated during the second stage is less than that generated during the first stage. Thus the asymptotic methods underestimate the energy of continuum radiation by a large amount when the propagation distance is not long enough, as in the case considered here.

Even though the asymptotic calculations of the radiation energy, E_{rad}, do not yield its value accurately enough, they still provide a solution to the following key question: How rapidly will this energy decrease with the decrease of β_3? We answer this question here, while moving the mathematical details of estimating the amount of continuum radiation to Appendix A. As is well known in the case of the NLS soliton, and as we also show in Appendix A to be the case for the DM soliton, E_{rad} is proportional to the value of the soliton's spectral power, $|\hat{u}_0(\omega)|^2$, at a certain frequency $\omega = \omega_r$:

$$E_{\mathrm{rad}} \approx \frac{\epsilon z \mu^2 \omega_r^5 |\hat{u}_0(\omega_r)|^2}{(3\mu\omega_r + D_0)}. \tag{29}$$

As discussed above and as Fig. 4(b) shows, this energy increases linearly with z. The physical reason for the occurrence of ω_r in relation (29) is that, at this frequency, the dispersion curves of the soliton and the linear radiation intersect,[16] thus leading to the energy transfer from the soliton to the continuum radiation at this frequency. In the spectral domain, generation of the continuum radiation is manifested by a small and narrow peak at $\omega = \omega_r$ (see, e.g., Fig. 3 of Ref. 15). As shown in Appendix A, ω_r is the real root of the cubic equation

$$\mu\omega_r^3 + \frac{D_0}{2}\omega_r^2 = -\frac{a_0^2}{\sqrt{2}}\left(I_0 - \frac{I_2}{4}\right), \tag{30}$$

where the integrals I_0 and I_2 are defined by Eq. (13). In Fig. 5 we plot the normalized radiation frequency ($\omega_r \tau_0$) as a function of $\beta_3/\beta_3^{1\%}$ for five values of dispersion strength S. For simplicity, in Fig. 5 and below we consider only the case of an idealized lossless fiber because this is sufficient to illustrate the main idea of our approach. Given the parameters of a realistic fiber such as the loss coefficients and the lengths of the two sections of the dispersion map,[13] we can always generalize the present results to a specific amplification scheme.

The following important trend is obvious from Fig. 5: For weak and moderately strong maps ($S < 2$), ω_r varies as β_3^{-1}. Therefore, as β_3 decreases, the radiation energy also decreases in proportion to the soliton's spectral power at ω_r, i.e., approximately exponentially fast. On the other hand, for stronger maps ($S > 3$), the radiation frequency remains almost constant as β_3 changes in the range $\beta_3^{1\%}/5$–$\beta_3^{1\%}$, and therefore the radiation energy in that case decreases simply as β_3^2 [cf. relation (29)].

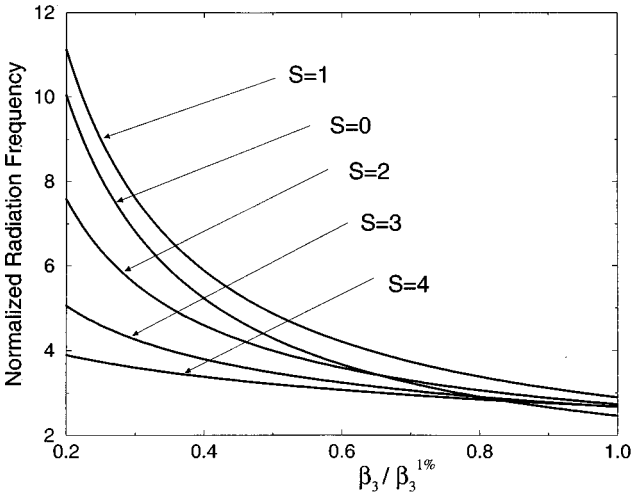

Fig. 5. Normalized radiation frequency $|\omega_r|\tau_0$ as a function of the TOD parameter for five values of the DM strength S.

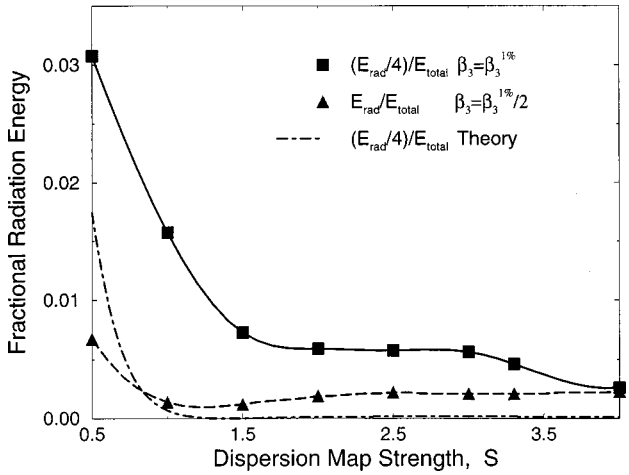

Fig. 6. Numerically calculated ratio of the radiation energy to the total DM soliton energy as a function of S at $Z = 300L_{\mathrm{map}}$ for $\beta_3 = \beta_3^{1\%}$ and $\beta_3 = \beta_3^{1\%}/2$. The additional factor of (1/4) is included in the data for $\beta_3 = \beta_3^{1\%}$ to demonstrate that for large values of S the radiation energy scales as β_3^2, as predicted in Subsection 4.D. Dashed and solid curves provide a cubic spline to the discrete data. The dotted–dashed curve shows the analytical estimate for the radiation energy in the lossless case as obtained from relation (29).

Thus, as β_3 is decreased from $\beta_3^{1\%}$ to, say, $\beta_3^{1\%}/2$, we should expect a much stronger suppression of the continuum radiation for not-too-strong maps. That this in fact occurs is confirmed by the numerical results shown in Fig. 6, where we plot the fractional radiation energy as a function of map strength S for two values of the TOD coefficient, $\beta_3 = \beta_3^{1\%}$ and $\beta_3 = \beta_3^{1\%}/2$. Note that for $S = 4$, when the radiation frequency ω_r is almost the same for $\beta_3 = \beta_3^{1\%}$ and for $\beta_3 = \beta_3^{1\%}/2$ (cf. Fig. 5), the radiation energy indeed scales as β_3^2 (recall the factor 1/4 used for the solid curve), in agreement with our prediction above. In Fig. 6 we also plot the ratio of the continuum radiation energy E_{rad} to the total soliton energy evaluated from Eqs. (28)–(30) for $\mu = \mu^{1\%}(S)$. The analytical formula is seen to underestimate greatly the radiation energy, the reason for which was given above.

From Fig. 6 we draw the following important conclusion: When $\beta_3 = \beta_3^{1\%}/2$, the total energy lost by a DM soliton into generation of both the continuum radiation and higher-order HG components is less than or approximately 1%. This condition,

$$\beta_3 \leqslant 1/2\beta_3^{1\%}(S), \tag{31}$$

is the main result of our study. When it is satisfied, the effect of TOD on a DM soliton (apart from the position shift) is negligible for transoceanic distances of propagation. Condition (31) is rather conservative; i.e., for sufficiently strong maps (e.g., $S > 2$) we can neglect both the TOD-induced radiation and the higher-order HG components for somewhat larger values of β_3 (cf. Fig. 6). We also emphasize that condition (31) was established on the basis of numerical calculations of the radiation energy, because the corresponding analytical calculations do not seem feasible, as explained above. We can suggest an analogy between this condition and the numerically derived condition under which TOD does not affect NLS solitons in a uniform-dispersion fiber.[22] The latter condition is, in fact, more restrictive than our condition (31), as it requires that the continuum radiation not be seen in numerical simulations performed with a certain precision.

We conclude this section by pointing out that generation of continuum radiation leads to a shift of the soliton's central frequency.[17,20,22] This effect is sometimes called spectral recoil because its origin lies in the conservation of the total momentum, defined by Eq. (A7) below. Inasmuch as the length of the shelf formed by the continuum radiation increases linearly in z [cf. Fig. 4(a) and the text after Eq. (A6) in Appendix A], so does the momentum carried by the radiated waves; hence the central frequency of the soliton should also shift, in the direction away from ω_r and at a constant rate (for sufficiently large z). This rate is given by relation (A9) below, and its normalized value $(\dot{\omega}_{\mathrm{sol}}\tau_0/I_0)$ is plotted in Fig. 2 as curve (a). In obtaining that curve we approximated $\hat{u}_0(\omega)$ by a two-term truncation (with $n = 0$ and $n = 4$) of Eq. (A2).

5. DISCUSSION AND CONCLUSIONS

In this section, we first summarize and interpret the results obtained above. Then we discuss the possibility of the existence of a nonradiating, weakly asymmetric DM soliton in the presence of TOD.

We have shown, by means of numerical simulations, that the energy lost by a DM soliton propagating in the presence of TOD into both the continuum radiation and higher-order HG components remains less than 1%, provided that condition (31) is satisfied. This condition may be thought of as an analog of the condition under which TOD does not affect a NLS soliton in a uniform-dispersion fiber,[22] although the latter condition is more restrictive, as was noted in Subsection 4.D. Another difference between the two conditions is that, in the uniform-dispersion case, the condition was formulated (after an appropriate normalization) in the form

$$\beta_3 < \text{number}.$$

In the DM case the map strength S is the additional parameter, and therefore the corresponding condition has to have the form

$$\beta_3 < \text{function of } S.$$

Taking that function of S as being related to the size of the largest symmetry-breaking HG component of the DM soliton appears to be a reasonable choice, because this automatically guarantees that the TOD-induced frequency and position shifts, as well as higher-order HG components, should remain small, too. Let us note that numerical results of Ref. 6 indicate that a single DM soliton could propagate over long distances even for $\beta_3 \approx 6.5\beta_3^{1\%}$, at least for the parameters used in that study (in our notation, those parameters were $\epsilon = 0.16$, $S = 4.2$, and $z_{\max} = 150$). However, as we verified, in that case a significant amount of energy is found outside the main peak of the pulse, as was also illustrated in Fig. 3 of Ref. 7 for slightly different values of the parameters. It is not clear how such a pulse might behave in collisions with pulses from other wavelength channels or interact with neighboring pulses that are similarly affected by TOD. Thus we believe that it is still advantageous to ensure that the energy in the continuum radiation and higher-order HG components be sufficiently small.

A realistic soliton-based dispersion management system is likely to use both optical filters and many wavelength channels. In this case it may be possible to suppress the dispersive waves that are generated as a result of TOD.[21] In fact, if, for a given channel, the radiation frequency ω_r falls outside the filter half-bandwidth $\omega_f/2$, and is still small enough not to fall into the bandwidth of the neighboring channel, i.e., if

$$\omega_f/2 < \omega_r < \omega_{\mathrm{ch}} - \omega_f/2, \tag{32}$$

where ω_{ch} is the channel spacing, the linear radiation can be effectively suppressed by optical filters. Then the condition on the allowed magnitude of TOD can be somewhat relaxed compared with condition (31). Note that TOD-induced frequency shifts, which originate from spectral recoil as well as from generation of the third-order HG component, can also be suppressed by the filters.

The shift of the soliton's position, given by Eq. (21), cannot be suppressed by optical filters. Although by itself this shift is harmless in the sense that it does not cause timing jitter, provided that the widths of all pulses in the same channel are the same, it can cause timing jitter when we account for the amplifier's noise. The amplified spontaneous emission generates amplitude fluctuations that change the pulse widths in a random way, thus causing each pulse to change its velocity randomly.[23] This kind of timing jitter for the NLS case was shown in Ref. 23 to dominate the Gordon–Haus jitter when the pulse width became sufficiently small.

In the remaining part of this section we discuss the relation of our results to those of a recent paper[24] in which a nonradiating DM soliton was numerically found even in the presence of TOD. In Ref. 24 it was also noted that a certain relation between the TOD coefficient and the parameters of the DM soliton had to hold for this to occur, but that relation was not specified. Here we point out

that the existence of a nonradiating DM soliton indeed follows from our relation (29); that is, when radiation frequency ω_r is such that the DM soliton's power spectrum at that frequency, $|\hat{u}(\omega_r)|^2$, vanishes, the soliton will not radiate.

We emphasize two points regarding this observation. First, such a nonradiating DM soliton can exist only when the map strength exceeds a certain threshold value, which can be estimated as follows: If one truncates expansion (A2) for $\hat{u}_0(\omega)$ at the term $n = 4$ (recall also that $a_2 = 0$), then the condition for such a truncated $\hat{u}_0(\omega)$ to become zero can be shown to be $a_4 \leqslant 0$. The amplitude $a_4(S)$ can be computed along the lines of Ref. 12, where in the lossless case it was found that $a_4 = 0$ for $S \approx 0.91$. Note that, when S is increased sufficiently above that value, terms with higher n need to be retained in expansion (A2), and $\hat{u}_0(\omega)$ can become zero at several points (on the real ω axis). However, the case when ω_r coincides with the first zero, ω_1, of the power spectrum, appears to be the most interesting. In the case of a lossless fiber, we verified that the location of ω_1 is predicted from expansion (A2) truncated at $n = 4$ with an accuracy better than 2% for $S < 2$ and better than 5% for $S < 3.5$.

It is also interesting to note that the same reason, i.e., the coalescence of the radiation frequency with the frequency where the pulse's power spectrum vanishes, may be behind the existence of a two-peak nonradiating soliton in a uniform-dispersion fiber, which was predicted and numerically observed in Ref. 25. In that paper, the existence of such a pulse was explained by destructive interference of the TOD-induced shelves in the time domain.

Our second remark is that a nonradiating DM soliton in the presence of TOD can be observed in either numerical simulations or real systems only when the asymptotic limit $z \to \infty$, for which relation (29) was derived, is reached. In fact, our own numerical simulations, whose details were presented in Subsection 4.C, did not show the existence of such a soliton. We performed simulations for several values of S in the range from 1 to 2. In particular, we considered the case $S = 1.41$, when $\omega_r = \omega_1$ for $\beta_3 = \beta_3{}^{1\%}$. (The value of β_3 for which ω_r equals ω_1 increases monotonically with S.) Decreasing the step size in z, increasing the number of points in τ, or both did not change our conclusion. How can one reconcile our numerical results with the results of Ref. 24 and the analytical prediction of relation (29)? Our answer is that relation (29) is valid only asymptotically, i.e., for $z \to \infty$. For z not sufficiently large, the pulse emits a considerable amount of radiation that is not accounted for by that relation [cf. the discussion related to Figs. 4(a) and 6]. We can further estimate, by generalizing the analysis presented in Appendix A, that for ω_r such that $\hat{u}_0(\omega_r) = 0$, the amplitude of the radiation far behind the soliton; i.e., for $|\tau| \gg \epsilon z$, decays as $(\epsilon\beta_3 z)^{-1/4}$, i.e., very slowly. In particular, it is not expected to decay much for the parameters $\epsilon = 0.2$, $\beta_3 \approx \beta_3{}^{1\%}$, and $z \approx 300$, which we used in our numerical simulations. In fact, we continued the simulations as far as $z = 800$ but still did not observe the asymptotic nonradiating soliton. On the other hand, the authors of Ref. 24 used a modified version of the accelerated convergence procedure, which was first proposed in Ref. 3 for TOD-free DM solitons. That procedure effectively increases the propagated distance z and thus is capable of finding asymptotically nonradiating DM solitons. A more detailed analysis of this issue requires a separate investigation. However, it does appear from this discussion that a nonradiating DM soliton is not likely to form in a real transmission system (with TOD) whose length is below 10,000 km.

APPENDIX A: ENERGY OF THE THIRD-ORDER DISPERSION–INDUCED CONTINUUM RADIATION

The derivation of the asymptotic expression for the energy of continuum radiation $E_{\rm rad}$ generated by a DM soliton in the presence of TOD closely follows similar derivations for the NLS soliton.[16,17,20] We stress that this derivation produces an accurate estimate of $E_{\rm rad}$ only in the asymptotic limit $z \to \infty$; see also Subsection 4.D, where this issue is discussed in detail. We start by substituting $u = u_0 + u_r$ into Eq. (5), where u_0 is the unperturbed DM soliton [Eq. (7)] and u_r is the radiation field to be determined. Because the radiation is both small and generated sufficiently far from the soliton's center [cf. Fig. 4(a)], we can neglect the terms that are nonlinear in u_r as well as the cross terms $|u_0|^2 u_r$ and $u_0{}^2 u_r{}^*$. Denoting the Fourier transform by $\hat{u}(\omega) = \int_{-\infty}^{\infty} \exp(-i\omega\tau) u(\tau) \mathrm{d}\tau$, we obtain

$$i\hat{u}_{r,z} - \left\{ \frac{\omega^2}{2}[D(z) + \epsilon D_0] + \epsilon\mu\omega^3 \right\} \hat{u}_r = \epsilon\mu\omega^3 \hat{u}_0, \tag{A1}$$

where, from Eq. (9), we have

$$\hat{u}_0(\omega) = \frac{\tau_0}{\sqrt{2\pi}} \exp\left[-\frac{1}{2}(\omega\tau_0)^2(1 + i\delta) \right] \times \sum_{n=0}^{\infty} (-1)^{3n/2} a_n H_n(\omega\tau_0). \tag{A2}$$

Solving Eq. (A1) and taking the inverse Fourier transform of the solution, we find that

$$u_r(\tau, z) = -\frac{\mu \exp(i\epsilon z k_{\rm sol})}{2\pi} \int_{-\infty}^{\infty} \omega^3 \hat{u}_0(\omega) \frac{\exp(i\omega\tau) - \exp[i\omega\tau - i\epsilon z(\mu\omega^3 + D_0\omega^2/2 + k_{\rm sol})]}{k_{\rm sol} + \mu\omega^3 + D_0\omega^2/2} \mathrm{d}\omega, \tag{A3}$$

where $k_{\rm sol}$ represents the nonlinear contribution to the soliton's propagation constant:

$$k_{\rm sol} = \epsilon \frac{|a_0|^2}{\sqrt{2}} \left(I_0 - \frac{I_2}{4} \right) \tag{A4}$$

[cf. Eq. (12)]. The integral in Eq. (A3) can be evaluated analytically only if some approximations are made. For large z, the main contribution to the integral in Eq. (A3) comes from the vicinity of $\omega = \omega_r$, where the denominator of the integrand vanishes. The corresponding value ω_r satisfies Eq. (30). By expanding the denominator in Eq. (A3) about ω_r and then using the formula

$$\int_{-\infty}^{\infty} \frac{f(\omega)\exp(i\omega\tau)}{\omega - \omega_0}\,\mathrm{d}\omega = \pi i f(\omega_0)\exp(i\omega_0\tau)\,\mathrm{sgn}(\tau) + O[\exp(-|\tau|)], \tag{A5}$$

while omitting the localized terms $O[\exp(-|\tau|)]$, we obtain the final result:

$$u_r(\tau, z) = -\frac{i\mu\omega_r{}^3\hat{u}_0(\omega_r)\exp(i\epsilon z k_{\mathrm{sol}} + i\omega_r\tau)}{2(3\mu\omega_r{}^2 + D_0\omega_r)} \times\{\mathrm{sgn}(\tau) - \mathrm{sgn}[\tau - \epsilon z(3\mu\omega_r{}^2 + D_0\omega_r)]\} + O(z^{-1/2}). \tag{A6}$$

The first term of this solution describes a shelf that extends away from the soliton over the region $0 < \tau < \tau_r$, with the shelf-length τ_r growing at a rate $d\tau_r/dz = \epsilon(3\mu\omega_r{}^2 + D_0\omega_r)$. The energy contained in this shelf, i.e., $\int_0^{\tau_r}|u_r|^2\mathrm{d}\tau$, is given by relation (29).

As was pointed out in Subsection 4.D, the generation of continuum radiation by the soliton leads to a shift of its central frequency[17] ω_{sol}, which can be estimated as follows: The evolution of u governed by Eq. (5) conserves the total momentum

$$P = \int_{-\infty}^{\infty}\left(u^*\frac{\partial u}{\partial\tau} - u\frac{\partial u^*}{\partial\tau}\right)\mathrm{d}\tau. \tag{A7}$$

Substituting $u = u_0 + u_r$ into Eq. (A7) and using the orthogonality of the radiation field u_r to the soliton u_0, we find that

$$\omega_{\mathrm{sol}}\int_{-\infty}^{\infty}|u_0|^2\mathrm{d}\tau \approx -\omega_r\int|u_r|^2\mathrm{d}\tau. \tag{A8}$$

Using the approximate form $\int_{-\infty}^{\infty}|u_0|^2\mathrm{d}\tau \approx a_0{}^2T_0\sqrt{\pi}$ for the total DM soliton energy and relation (29) for the radiation energy, we obtain

$$\frac{\mathrm{d}\omega_{\mathrm{sol}}}{\mathrm{d}z} \approx -\frac{\epsilon\mu^2\omega_r{}^6|\hat{u}_0(\omega_r)|^2}{a_0{}^2T_0\sqrt{\pi}(3\mu\omega_r + D_0)}. \tag{A9}$$

ACKNOWLEDGMENTS

The research is supported in part by the National Science Foundation under grant PHY94-15583. That of T. I. Lakoba is also supported in part by U.S. Office of Naval Research grant N00014-98-1-0630. We are grateful to K. Kikuchi for providing Ref. 24 before its publication. We thank the anonymous referees for useful suggestions.

T. I. Lakoba's e-mail address is lakobati@optics.rochester.edu; G. P. Agrawal's e-mail address is gpa@optics.rochester.edu.

REFERENCES

1. A. Hasegawa, Y. Kodama, and A. Maruta, "Recent progress in dispersion-managed soliton transmission technologies," Opt. Fiber Technol.: Mater., Devices Syst. **3**, 197 (1997); J. F. L. Devaney, W. Forysiak, A. M. Niculae, and N. J. Doran, "Soliton collisions in dispersion-managed wavelength-division-multiplexed systems," Opt. Lett. **22**, 1695 (1997); R.-M. Mu, V. S. Grigoryan, C. R. Menyuk, E. A. Golovchenko, and A. N. Pilipetskii, "Timing-jitter reduction in a dispersion managed soliton system," Opt. Lett. **23**, 930 (1998); I. Morita, K. Tanaka, N. Edagawa, S. Yamamoto, and M. Suzuki, "40 Gbit/s single-channel soliton transmission over 8600 km using periodic dispersion compensation," Electron. Lett. **34**, 1863 (1998).
2. N. J. Smith, N. J. Doran, F. M. Knox, and W. Forysiak, "Energy-scaling characteristics of solitons in strongly dispersion-managed fibers," Opt. Lett. **21**, 1981 (1996).
3. J. H. B. Nijhof, N. J. Doran, W. Forysiak, and F. M. Knox, "Stable soliton-like propagation in dispersion-managed systems with net anomalous, zero, and normal dispersion," Electron. Lett. **33**, 1726 (1997).
4. A. Berntson, N. J. Doran, W. Forysiak, and J. H. B. Nijhof, "Power dependence of dispersion-managed solitons for anomalous, zero, and normal path-average dispersion," Opt. Lett. **23**, 900 (1998).
5. M. Suzuki, I. Morita, N. Edagawa, S. Yamamoto, and S. Akiba, "20 Gbit/s-based soliton WDM transmission over transoceanic distances using periodic compensation of dispersion and its slope," Electron. Lett. **33**, 691 (1997); M. Suzuki, I. Morita, N. Takeda, N. Edagawa, S. Yamamoto, and S. Akiba, "160 Gbit/s (8 × 20 Gbit/s) soliton WDM transmission experiments using dispersion flattened fiber and dispersion compensation," Electron. Lett. **34**, 475 (1998).
6. K. Hizanidis, B. A. Malomed, H. E. Nistazakis, and D. Frantzeskakis, "Stabilizing soliton transmission by third-order dispersion in dispersion-compensated fiber links," Pure Appl. Opt. **7**, L57 (1998).
7. K. Hizanidis, B. A. Malomed, H. E. Nistazakis, and D. Frantzeskakis, "Variational approach to transmission in DM long optical links," in *New Trends in Optical Soliton Transmission Systems*, A. Hasegawa, ed. (Kluwer Academic, Dordrecht, The Netherlands, 1998).
8. X. Wang, Y. Takushima, and K. Kikuchi, "Performance restriction from third-order dispersion in long-distance high-speed dispersion-managed IM/DD systems," presented at the Optoelectronics and Communications Conference, Japan (1998); M. Suzuki, N. Edagawa, N. Takeda, K. Imai, S. Yamamoto, and S. Akiba, "20 WDM, 10.66 Gbit/s transmission experiment over 9000 km using periodic dispersion slope compensation," Electron. Lett. **34**, 479 (1998).
9. T. I. Lakoba and D. J. Kaup, "Shape of stationary soliton in strong dispersion management regime," Electron. Lett. **34**, 1124 (1998).
10. S. K. Turitsyn and V. K. Mezentsev, "Dynamics of a self-similar dispersion-managed soliton presented in the basis of chirped Gauss–Hermite functions," JETP Lett. **67**, 640 (1998).
11. S. K. Turitsyn, T. Schäfer, and V. K. Mezentsev, "Self-similar core and oscillatory tails of a path-averaged chirped dispersion-managed optical pulse," Opt. Lett. **23**, 1351 (1998).
12. T. I. Lakoba and D. J. Kaup, "A Hermite–Gaussian expansion for pule propagation in strongly dispersion-managed fibers," Phys. Rev. E **58**, 6728 (1998).
13. T. I. Lakoba, J. Yang, D. J. Kaup, and B. A. Malomed, "Conditions for stationary pulse propagation in the strong dispersion management regime," Opt. Commun. **149**, 366 (1998).
14. Y. Kodama, "Nonlinear chirped RZ and NRZ pulses in optical transmission lines," preprint (Osaka University, Osaka, Japan); V. S. Grigoryan and C. R. Menyuk, "Dispersion-managed solitons at normal average dispersion," Opt. Lett. **23**, 609 (1998).
15. P. K. A. Wai, H. H. Chen, and Y. C. Lee, "Radiation by solitons at the zero group-velocity-dispersion wavelength of

single-mode optical fibers," Phys. Rev. A **41**, 426 (1990).
16. V. I. Karpman, "Radiation by solitons due to higher-order dispersion," Phys. Rev. E **47**, 2073 (1993).
17. N. Akhmediev and M. Karlsson, "Cherenkov radiation emitted by solitons in optical fiber," Phys. Rev. A **51**, 2602 (1995).
18. G. P. Agrawal, *Nonlinear Fiber Optics* (Academic, San Diego, Calif., 1995), p. 47.
19. Y. Kodama, A. V. Mikhailov, and S. Wabnitz, "Input pulse optimization in wavelength-division-multiplexed soliton transmission," Opt. Commun. **143**, 53 (1997).
20. J. N. Elgin, T. Brabec, and S. M. J. Kelly, "A perturbative theory of soliton propagation in the presence of third-order dispersion," Opt. Commun. **114**, 321 (1995).
21. I. M. Uzunov, M. Gölles, and F. Lederer, "Soliton interaction near the zero-dispersion wavelength," Phys. Rev. E **52**, 1059 (1995).
22. P. K. A. Wai, C. R. Menyuk, H. H. Chen, and Y. C. Lee, "Effect of axial inhomogeneity on solitons near the zero dispersion point," IEEE J. Quantum Electron. **24**, 373 (1988).
23. J. D. Moores, W. S. Wong, and H. A. Haus, "Stability and timing maintainance in soliton transmission and storage rings," Opt. Commun. **113**, 152 (1994); R.-J. Essiambre and G. P. Agrawal, "Timing jitter of ultrashort solitons in high-speed communication systems. I. General formulation and application to dispersion-decreasing fibers," J. Opt. Soc. Am. B **14**, 314 (1997).
24. Y. Takushima, X. Wang, and K. Kikuchi, "Transmission of 3-ps dispersion-managed soliton pulses under influence of third-order dispersion," Electron. Lett. **35**, 739 (1999).
25. M. Klauder, E. W. Laedke, K. H. Spatschek, and S. K. Turitsyn, "Pulse propagation in optical fibers near the zero-dispersion point," Phys. Rev. E **47**, R3844 (1993).